The M, E, and N structural proteins of the severe acute respiratory syndrome coronavirus are required for efficient assembly, trafficking, and release of virus-like particles.

Y. L. Siu, K. T. Teoh, J. Lo, C. M. Chan, F. Kien, N. Escriou, S. W. Tsao, J. M. Nicholls, R. Altmeyer, J. S. M. Peiris, et al.

JVI Accepts, published online ahead of print on 27 August 2008
J. Virol. doi:10.1128/JVI.01052-08

The M, E and N structural proteins of the SARS coronavirus are required for efficient assembly, trafficking and release of virus-like particles.

Siu YL.[1], Teoh KT.[1], Lo J.[2], Chan CM.[3], Kien F.[1], Escriou N.[4], Tsao SW.[5], Nicholls JM.[2], Altmeyer R.[6], Peiris JS.[1,3], Bruzzone R.[1] and Nal B.[1,7]

From the [1] HKU-Pasteur Research Centre, 8 Sassoon Road, Hong Kong SAR, China; [2] Department of Pathology, The University of Hong Kong, Queen Mary Hospital, Hong Kong SAR, China; [3] Department of Microbiology, The University of Hong Kong, 21 Sassoon Road, Hong Kong SAR, China; [4] Institut Pasteur, Unité de Génétique Moléculaire des Virus Respiratoires, URA-CNRS 3015, 25-28 Rue du Docteur Roux, 75724, Paris Cedex 15, France; [5] Department of Anatomy; The University of Hong Kong, 21 Sassoon Road, Hong Kong SAR, China; [6] CombinatoRx-Singapore Pte Ltd, 11 Biopolis Way, 138667 Singapore.

[7] To whom correspondence should be addressed: e-mail: bnal@hku.hk
Tel: (852)-2816-8403 / Fax: (852)-2872-5782

Abstract

Production of virus-like particles (VLPs) constitutes a relevant and safe model to study molecular determinants of virion egress. The minimal requirement for assembly of VLPs for the coronavirus responsible for severe acute respiratory symdrome in humans (SARS-CoV) is still controversial. Recent studies have described that SARS-CoV VLP formation depends on either M and E or M and N proteins. Here we show that both E and N must be co-expressed with M for efficient production and release of VLPs by transfected Vero E6 cells. This result suggests that the mechanism of SARS-CoV assembly differs from other studied coronaviruses, which only require M and E for VLP formation. When co-expressed, the native envelope trimeric S glycoprotein is incorporated onto VLPs. Interestingly, when a fluorescent protein tag is added to the C-terminal end of N or S, but not M, the chimeric viral proteins can be assembled within VLPs and allow visualization of VLP production and trafficking in living cells by state of the art imaging technologies. Fluorescent VLPs will be used further to investigate the role of cellular machineries during SARS-CoV egress.

Keywords: SARS coronavirus, virus-like particle, virus assembly, virus budding, egress, fluorescent viral particles

Introduction

Coronaviruses are positive-sense RNA enveloped viruses that belong to the *Coronaviridae* family in the Nidovirales order. These viruses are found in a wide variety of animals and can cause respiratory and enteric disorders of diverse severity (15, 18). In the past five years, several human and animal coronaviruses have been discovered, including the highly pathogenic virus responsible for the severe acute respiratory syndrome (SARS-CoV) (34, 58, 60, 64, 68, 69). Coronavirus particles consist of a helical nucleocapsid structure, formed by the association between nucleocapsid (N) phosphoproteins and the viral genomic RNA, which is surrounded by a lipid bilayer where three or four types of structural proteins are inserted: the spike (S), the membrane (M), the envelope (E) proteins and, for some coronaviruses only, the hemagglutinin-esterase (HE) protein (see for review: (12). Once sufficient amounts of new genomic RNA and structural proteins have been produced, assembly of particles occurs. Assembly and release of virions are the last stages of the virus life cycle.

The triple spanning membrane glycoprotein M drives assembly of coronavirus, which bud into the lumen of the endoplasmic reticulum-Golgi intermediary compartment (ERGIC) (32, 33, 62, 63). M is the most abundant envelope protein that sorts viral components to be incorporated into virions. M oligomerisation, mainly driven by its transmembrane domain, is believed to allow formation of a lattice of M proteins at ERGIC membranes (14, 41). S and E membrane proteins are integrated into the lattice through lateral interactions with M, whereas N and viral RNA interact with M C-terminal domain, which is exposed to the cytosol (4, 8, 13, 19, 30, 36, 48, 54, 55). The coronavirus S protein, responsible for receptor

binding and membrane fusion, does not seem to have any major role in coronavirus assembly. Recent studies show that E is a viroporin that forms ion channels (46, 66, 67). Despite its minor incorporation into virion particles (7, 22, 40), the small E protein plays an important but not fully understood role in virus morphogenesis and budding (20, 35, 70). Studies performed on coronaviruses, including the SARS-CoV, demonstrate that depletion of the E gene from coronavirus genome strongly diminish virus growth and particle formation (9, 16, 35, 37, 57). The N protein self-associates and encapsidates the RNA genome for incorporation into budding virions through interactions with the M protein independently of E and S proteins (24, 52, 53, 61). For SARS-CoV, the interaction of N with M was described to be independent of viral RNA (25, 45).

Work on mouse hepatitis virus (MHV), bovine coronavirus (BcoV), infectious bronchitis virus (IBV) and transmissible gastroenteritis virus (TGEV) has established that E and M proteins are necessary and sufficient for assembly of virus-like particles (VLPs), which share size and morphological features with real viruses (1, 2, 7, 8, 38, 65). Nevertheless, the minimal requirement for assembly of SARS-CoV VLPs is still controversial. Huang Y. and colleagues described formation of VLPs in transfected human 293 renal epithelial cells that only required co-expression of the M and N viral proteins (29). On the contrary, other studies described that co-expressed M and E proteins were sufficient for release of sedimentable particles from transfected mammalian cells (27) or insect cells, using a baculovirus expression system (26, 50). A few groups have proposed immunization with SARS-CoV VLPs as an effective vaccine strategy. VLPs produced in insect cells or chimeric MHV/SARS-CoV VLPs produced in mammalian cells were used in these studies (42, 44).

100 Our objective was to delineate the molecular mechanisms that regulate SARS-
101 CoV egress in mammalian cells. Here we demonstrate that whereas VLPs could
102 hardly be recovered from culture medium of cells co-expressing combinations of M
103 and E or M and N proteins, co-expression of both SARS-CoV E and N with M
104 allowed release of significant levels of VLPs within one day. When co-expressed,
105 the trimeric S protein was found in VLPs. Therefore, in apparent contrast to other
106 coronaviruses, SARS-CoV egress strongly depends on three structural proteins:
107 M, E and N. Addition of fluorescent tags to viral structural proteins allowed us to
108 visualize egress of fluorescent VLPs in living cells. Monitoring of VLPs egress in
109 living cells will be a powerful new tool to study the involvement of viral and cellular
110 factors during the late stages of the SARS-CoV life cycle.
111

Materials and Methods

Cells and culture conditions. The Vero E6 African Green Monkey kidney cell line was cultured in Dulbecco's modified Eagle's medium supplemented with 10% heat-inactivated foetal calf serum, 100 U of penicillin and 100 g of streptomycin per ml, at 37°C with 5% CO_2.

Plasmid constructions. CDNAs coding for the SARS-CoV M, E, S and N structural proteins were codon-optimized for mammalian cells and synthesized by GeneArt (Regensburg, Germany). The M cDNA was amplified by PCR and sub-cloned into the pIRES plasmid vector (BD Biosciences, San Jose, CA, USA) between the Nhe I and EcoR I restriction sites of the upstream multiple cloning site. The E cDNA was amplified by PCR and inserted either into the pcDNA3.1 plasmid vector between the Kpn I and Not I restriction sites or into the pIRES plasmid vector between the Sal I and Not I restriction sites of the downstream multiple cloning site. The S cDNA was amplified by PCR and inserted either into the pcDNA3.1 plasmid vector between the Nhe I and Apa I restriction sites. The pcDNA-Nflag plasmid was constructed from the original pCRScript-Nflag (produced by GeneArt, Regensburg, Germany) using the Kpn I and Xho I restriction sites. The Flag tag was in fusion with the 3' end of N cDNA and separated from N cDNA by six nucleotides encoding two glycine residus. The cDNAs coding for the enhanced yellow (eYFP), cyan (eCFP), green (eGFP) fluorescent proteins and the monomeric red fluorescent protein (mRFP1, (5), were amplified by PCR from plasmids purchased from Clontech Laboratories (Takara Bio, Shiga, Japan) and subcloned into pcDNA3.1 or pIRES vectors. Then S, N or

137 M cDNAs were inserted in 5' of the fluorescent protein cDNAs using Cla I and Apa
138 I sites (S and N) or Xho I and Mlu I (M) restriction sites. The two fused cDNAs
139 were separated by two codons encoding glycines.
140
141 ***Antibodies.*** The M and E proteins were detected with rabbit polyclonal antibodies
142 raised against the C-terminal extremity of each protein. The rabbit polyclonal
143 antibody against the M C-terminal domain was purchased from ProSci
144 Incorporated (Poway, CA, USA). The rabbit polyclonal antibody against the E
145 protein was produced by Dr Nicolas Escriou (Institut Pasteur, Paris) using a C-
146 terminal peptide. The Flag tag was detected with the mouse monoclonal IgG1 M2
147 antibody purchased from Sigma-Aldrich. The mouse polyclonal antibody against
148 the S protein was obtained by immunizing mice with purified S trimers expressed
149 in mammalian cells as described previously (31). The mouse monoclonal antibody
150 against the N protein was a generous gift from Dr Chan KH (Department of
151 Microbiology, the University of Hong Kong) and produced as described in (56).
152
153 ***Transient transfections and production of SARS-CoV VLPs.*** Eight hundred
154 thousand cells were plated in 75 cm^2 dishes, incubated over-night and transfected
155 with plasmid constructs using the FuGENE 6 transfection reagent (Roche, Basel,
156 Switzerland), according to the manufacturer's instructions. Briefly, 54 μl of
157 FuGENE 6 transfection reagent were mixed with DMEM, incubated for five
158 minutes and then 6 μg of each plasmid were added. The FuGENE 6 / plasmid
159 mixture was incubated for 30 minutes at room temperature. Cell medium was
160 discarded and replaced with 3 ml of warm DMEM. The FuGENE 6 / plasmid
161 mixture was added to the cells. After 3 hours of incubation at 37°C, the medium

containing the transfection mixture was discarded and 10 ml of fresh medium was added. Cells were incubated for 21 or 45 hours.

Purification of SARS-CoV VLPs. At 24 or 48 hours post-transfection, cell medium was collected and cleared by centrifugation at low speed (1000g for 10 minutes) to pull-down cell debris. After passing through 0.45 μm filter, cleared cell medium were then loaded on top of 20% sucrose cushions and ultra-centrifuged for 3 hours at 28,000 rpm using a SW41 rotor (Belkman Coulter Inc, Fullerton, CA, USA). VLP-containing pellets were resuspended in Tris HCl 50 mM NaCl 100 mM EDTA 0.5 mM pH7.4 (TNE) buffer.

Western blot analysis of VLPs and cell lysates. For Western blot analysis of purified VLPs, 15 μl of resuspended pellets from ultracentrifuged culture medium were mixed with 5 μl lithium dodecyl sulfate (LDS)-containing loading buffer and loaded on 4 to12 % polyacrylamide gels (NuPAGE Novex Bis-Tris Mini Gels, Invitrogen, Carlsbad, CA, USA). Electrophoresis was performed with the NuPAGE MOPS SDS Running Buffer from the same manufacturer. Alternatively, resuspended pellets from 48 hours time points were loaded on top of 20 to 60% sucrose gradients and ultracentrifuged for 3.5 hours at 26,700 rpm (27). Twenty fractions were collected and analyzed by Western blot. For Western blot analysis of cell lysates, cells were washed twice with PBS 1X at 24 or 48 hours post-transfection, and lysed in lysis buffer containing 1% Triton X-100, 150 mM NaCl, 20 mM Tris-HCl pH7.5 and 1 mM EDTA for 15 minutes on ice with frequent vortexing. Then lysates were cleared by centrifugation at 16100 g for 15 minutes at 4^{o}C and analyzed by Western blot. 15 μl of each lysate were mixed with 5 μl

187 LDS loading buffer and loaded on polyacrylamide gels. For detection of E but S,
188 samples were treated with dithiothreitol and heated at 95°C for 5 minutes before
189 migration on polyacrylamide gels. To detect both E and trimers of S from same
190 preparations, samples were split and either treated or not before loading of two
191 separate gels for E and S detection, respectively. Results for M and Nflag were
192 similar with or without treatment.
193
194 ***Electron microscopy.*** For transmission electron microscopy experiments,
195 transfected cells were harvested at 24 and 48 hours post-transfection. Cells were
196 detached using 10 mM EDTA, fixed in 2.5 % glutaraldehyde in cacodylate buffer
197 and post-fixed with 1% Osmium Tetroxide (OsO_4) in Cacodylate buffer for 1 hour
198 at room temperature. Then cells were embedded in 2% agarose to form cell blocks
199 which were then dehydrated in graded series of ethanol and embedded in epoxy
200 resin. Ultrathin sections were stained for 45 minutes with 2% aqueous uranyl
201 acetate and for 30 minutes with Reynolds' lead citrate. For analysis of secreted
202 VLPs, VLPs were purified from cell medium by ultracentrifugation on 20% sucrose
203 cushion, separated on 20-60% discontinuous sucrose gradient and fraction 10 was
204 collected and then concentrated by ultracentrifugation in TNE buffer, pH 7.4 for
205 one hour at 28,000 rpm. 5µl of the VLP suspension, mixed with equal volume of
206 negative stain (2% aqueous uranyl acetate and 2% phosphotungstate solution, pH
207 7.0), was placed onto a formvar-carbon-coated copper grid for 2 minutes, excess
208 suspension were drained. The grids were viewed and photographed with a Philip
209 CM100 electron microscope at 80 kV.
210

Fluorescence microscopy. For fluorescence microscopy on fixed cells, Vero E6 cells were grown on glass coverslips, transfected and analyzed at 24 hours post-transfection. Cells were washed with PBS, nuclei were stained with DAPI and coverslips were mounted on glass slides for analysis. Fixed cells were visualized under AxioObserver Z1 inverted motorized fluorescent microscope using the ApoTome module and piloted through the Axiovision 4.6 software and images were acquired through the MRm AxioCam high resolution CCD camera (Carl Zeiss, Germany). For fluorescence microscopy on live cells, Vero E6 cells were grown in glass-bottom culture dish (MatTech, USA), transfected and analyzed at 24 hours post-transfection. Cells were washed and medium was changed to HBSS, Optimem pre-warmed culture medium. Widefield image acquisitions of live cells were obtained using the system described above. Confocal acquisitions of live cells were acquired at the Hong Kong University Core Imaging Facility using an AxioObserver Z1 inverted motorized fluorescent microscope equipped with a spinning disc confocal imaging system (UltraVIEW ERS, PerkinElmer, Shelton, CT, USA). For brefeldin A (BFA) treatment, cells were incubated with 6 μg per ml of BFA for indicated times. To release BFA effect, cells were washed three times in PBS 1X and reincubated in normal medium for indicated times.

Results

Efficient production and release of SARS-CoV VLPs are driven by co-expression of M, N and E structural proteins.

To determine the optimal conditions for efficient SARS-CoV VLP production, we chose to co-express different combinations of structural proteins in the Vero E6 African green monkey cell line, which is permissive to SARS-CoV replication (34). cDNAs encoding SARS-CoV structural proteins M, E and N were codon-optimized for expression in mammalian cells. Understanding the importance to maintain a low E/M ratio in transfected cells to ensure concomitant expression of E and M, low incorporation of E into VLPs and prevent potential formation of E-containing vesicles, we reasoned that the use of the pIRES bi-cistronic plasmid should be appropriate. This plasmid presents the double advantage to ensure co-expression of both cDNAs in transfected cell and allows a reduced rate of translation of the downstream gene by utilizing a partially disabled internal ribosome entry site (IRES) sequence. We therefore subcloned M upstream of E cDNA in the pIRES vector. N was expressed from a pcDNA plasmid with a C-terminal Flag tag. Vero E6 cells were either not transfected or transfected with pcDNA-E, pIRES-M or pIRES-M-E alone, pIRES-M plus pcDNA-Nflag and pIRES-M-E plus pcDNA-Nflag (Figure 1A). At 24 and 48 hours post-transfection culture medium and cells were harvested. Culture medium was subjected to ultracentrifugation on a 20% sucrose cushion to isolate VLPs and the SARS-CoV structural proteins assembled into VLPs were analyzed by Western blot.

The M protein was readily detected at both 24 and 48 hours post-transfection in lysates from Vero E6 cells transfected with pIRES-M, pIRES-M-E, pIRES-M plus

pcDNA-Nflag and pIRES-M-E plus pcDNA-Nflag (Figure 1A, upper panels). As described previously, three major forms of M, which correspond to different glycoforms, were detected on SDS-PAGE: two bands at ~ 18 and 28 KDa and a smear at higher molecular sizes reflecting heterogeneity of glycosylation patterns (51). As expected, higher levels of M were detected in cell lysates at 48 hours than at 24 hours post-transfection. Whereas a 10 KDa protein corresponding to E could be easily detected in cell lysates from cells transfected with pcDNA-E plasmid, its expression was much lower in cells transfected with the pIRES-M-E bi-cistronic vector. The Nflag protein was found in cell lysates from both pIRES-M plus pcDNA-Nflag and pIRES-M-E plus pcDNA-Nflag transfected cells at similar levels. A major band corresponding to a protein with an apparent molecular size of 45 KDa was detected.

Strikingly, the efficacy of VLP production was dramatically affected by the combination of viral proteins co-expressed (Figure 1A, lower panels). Although M was not detected in ultracentrifuged culture medium from pIRES-M, pIRES-M-E or pIRES-M plus pcDNA-Nflag transfected cells at 24 hours post-transfection, significant levels were found in preparations from pIRES-M-E plus pcDNA-Nflag transfected cells. Similarly, the N protein was only detected in ultracentrifuged culture medium from pIRES-M-E plus pcDNA-Nflag transfected cells at this early time point. Signals for E were below the limit of detection at 24 hours and detectable only at 48 hours. Finding low amounts of E in VLPs is in accordance with the minor presence of this protein in coronavirus particles, despite its important role for virion assembly and budding (9, 20, 37, 57, 65). In conclusion, only when M, E and N proteins were co-expressed, VLPs that contained the M and N proteins could be isolated from culture medium at 24 hours post-transfection.

At 48 hours post-transfection, E was found in ultracentrifuged culture medium from cells transfected with the pcDNA-E plasmid alone. This is in agreement with previously published data that describe secretion of E proteins independently of other viral elements (7, 47, 50). At this time point, trace amounts of M were detected in ultracentrifuged culture medium from pIRES-M and pIRES-M-E transfected cells, whereas significant levels of M and N were found for pIRES-M plus pcDNA-Nflag ultracentrifuged culture medium. Independent secretion of SARS-CoV M proteins from Vero E6 cells as well as production of M-E VLPs was described by Mortola and Roy (2004) at four days post-transfection. Production of SARS-CoV M-N VLPs has already been reported by Huang Y. and colleagues in transfected 293 renal epithelial cells at 63 hours post-transfection (29). Very interestingly, in our conditions, significantly higher levels of M and N proteins were found in purified VLPs from pIRES-M-E plus pcDNA-Nflag than pIRES-M plus pcDNA-Nflag transfected cells at 48 hours post-transfection. We were also able to detect E in these conditions, but not when cells were only transfected with the pIRES-M-E vector.

In order to verify that inefficacy of production of M-E VLPs by cells transfected with pIRES-M-E was not due to inefficient E expression, we performed similar experiments but expressed E from a pCDNA-E plasmid and analyzed cells and medium at 48 hours post-transfection (Figure 1B). As expected, higher levels of E were detected in lysates of cells transfected with pIRES-M plus pCDNA-E and pIRES-M plus pCDNA-E plus pCDNA-Nflag than pIRES-M-E and pIRES-M-E plus pCDNA-Nflag, respectively (Figure 1B, left panel). Nevertheless, neither production of M-E VLPs nor M-E-N VLPs were improved by increase of E expression (Figure 1B, right panel). On the contrary, production of M-E-N VLPs

was enhanced when the bicistronic vector was used, as indicated by higher levels of Nflag, M and E proteins secreted, and the ratio E(medium)/E(lysate) was significantly higher in these conditions. This result suggests that expression of E along with M from the pIRES-M-E bicistronic vector and in combination with N is favorable to the production of SARS-CoV VLPs.

We then investigated co-sedimentation of secreted viral structural proteins by performing sucrose gradient fractionation on ultracentrifuged cell medium. Cells were either transfected by individual plasmids or combinations of plasmids as described previously. In this experiment we used the individual plasmid for E expression to verify potential presence of E-containing vesicles in medium when E was expressed at higher levels. At 48 hours post-transfection, cleared cell medium was ultracentrifuged on 20% sucrose cushion and pellets were resuspended in TNE buffer. As controls, viral proteins contained in cell lysates and pellets from ultracentrifuged medium were analyzed by Western blot (Figure 1C, left panel). Pellets were loaded on top of 20-60% discontinuous sucrose gradients. After another round of ultracentrifugation, 20 fractions were collected and analyzed by Western blot (Figure 1C, right panels a to e). Results were consistent with the data described in Figure 1 A and B. When M was expressed alone, very little amounts of protein were found in cell medium and traces were detected in fraction 9 (Figure 1C, panel a). Coexpression with E or Nflag, allowed secretion of slightly higher levels of M in cell medium and detection of M in fractions 7 to 11, with enrichment in fraction 10 (Figure 1C, panel c) or 11 (Figure 1C, panel d), respectively. E protein was not detectable in fractions from medium of either pCDNA-E or pIRES-M plus pCDNA-E transfected cells (Figure 1C, panel b and c). Nflag cosedimented with M when co-expressed (Figure 1C, panel d). As expected, greater levels of M,

E and Nflag proteins were found in medium of cells expressing all three viral proteins (Figure 1C, panel e). M and Nflag were present in fractions 5 to 14 with proportional levels. E was detected in fractions 8 to 10 where M and N proteins were also enriched. Altogether, these results show that secreted viral structural proteins cosediment in sucrose gradient and therefore strongly suggest that viral proteins are associated into VLPs. Moreover, secretion of E-containing vesicles does not seem to be a major phenomenon in Vero E6 cells expressing E alone or in combination with other viral proteins in our system. Indeed, in all conditions, levels of E in cell medium were systematically low and only detected in fractions when co-expressed with M and N.

Altogether these data establish for the first time that all three M, E and N structural SARS-CoV proteins are important for efficient production and release of SARS-CoV VLPs.

S is incorporated onto SARS-CoV M-E-N-containing VLPs.

We then investigated whether the SARS-CoV S glycoprotein could be incorporated onto secreted M-E-N VLPs. S cDNA was codon optimized and subcloned in the pcDNA vector. Vero E6 cells were transfected with pIRES-M-E plus pcDNA-Nflag plus pcDNA-S. Protein expression was verified in cell lysates at 48 hours post-transfection (data not shown). To monitor association of S onto M-E-N VLPs, we performed sucrose fractionation on VLPs previously purified from culture medium (Figure 2). All S, Nflag, M and E proteins were co-sedimented and enriched in fractions 9 and 10 corresponding to ~40% sucrose. It is notable that S was mainly detected in its native trimeric form in these fractions (540 KDa), although we also detected low levels of monomers (180 KDa) and dimers (360

KDa), which may have resulted from sample treatment and SDS-PAGE conditions. Higher molecular weight proteins, detected with anti-S antibodies, were found in the lightest fractions 1 to 6. These forms could correspond to soluble, non-incorporated forms of S proteins that have formed aggregates. We have previously described formation of S aggregates in preparations of purified SARS-CoV S trimers from mammalian cell lysates (31). This result confirms association of all four SARS-CoV structural proteins into S-M-E-N VLPs that can be purified from culture medium of transfected cells.

VLPs bud into a perinuclear compartment and are transported within vesicles to the plasma membrane.

We next studied the subcellular localization of SARS-CoV VLPs by electron microscopy (Figure 3). pIRES-M-E plus pcDNA-Nflag plus pcDNA-S co-transfected Vero E6 cells were fixed at 24 and 48h post-transfection and ultrathin sections were prepared for transmission electron microscopy (Figure 3A to G). Large amounts of VLPs, with diameters ranging from 40 to 150 nm on sections, were found within the cytoplasm of positive cells. Three main patterns of subcellular localization were observed. First, VLPs were found within perinuclear compartments, which had appearance of groups of vacuoles (Figure 3A, C and D), or, alternatively but seldom observed, which presented morphological characteristics of the endoplasmic reticulum (Figure 3B). Vacuoles were observed at both 24 hours and 48 hours post-transfection with a diameter ranging from 300 nm to 1.5 μm on sections. Very interestingly, we detected several events of VLP budding at vacuole membranes (Figure 3D). Although VLPs accumulated therein, they were not highly compacted in this compartment. Moreover, VLPs appeared

pleiomorphic and heterogenous material was also observed (Figure 3D). Tubular structures were seen within some VLP-containing vacuoles, mainly at 24 hours post transfection (data not shown). Second, VLPs were observed in vesicles scattered in the cytoplasm (Figure 3A, B, C and E). These vesicles had a diameter ranging from 200 nm to 1 μm on sections and VLPs were more compacted inside. They could be found at proximity of the perinuclear VLP-containing compartments up to the cortical area. VLPs contained in these vesicles looked more homogenous in size and shape. Third, VLPs were occasionally found at the cell surface (Figure 3A, F and G). Although we could not observe obvious spike-like structures surrounding the VLP envelope, spike-like protuberances were occasionally detected (Figure 3G). Moreover, binding of VLPs to cell surface suggests the presence of spikes and receptor recognition. Some cells, in which very high amounts of VLPs were found, presented characteristics of apoptosis with fragmented nucleus and disrupted membranes (data not shown). The cytoplasm of these cells was filled up with VLPs, either free or within intracellular compartments. The morphology of released VLPs was investigated further by electron microscopy on negatively stained particles that were purified from cell medium (Figure 3F). Round-shaped particles with a diameter of 80-100 nm were readily observed. Again, we could not observe the typical corona of spikes around VLPs (21) but globular structures protruding from VLPs were detected, which likely corresponded to trimers of spikes. Altogether, our data suggest that SARS-CoV VLPs bud in an intracellular compartment of Vero E6 cells and are efficiently transported within vesicles to the plasma membrane where they are released. Shape and size of secreted VLPs are in accordance with the morphological characteristics of the

404 SARS-CoV and therefore these VLPs should be a safe and appropriate model to
405 study assembly and release of SARS-CoV virions.
406
407 **Assembly and release of VLPs that incorporate fluorescently-tagged**
408 **structural viral proteins.**
409 In order to visualize in real time, the assembly, trafficking and release of SARS-
410 CoV VLPs, we engineered plasmid constructs that allow expression of viral
411 proteins in fusion with fluorescent proteins. The pIRES-MmRFP1-E, pcDNA-
412 NeCFP and pcDNA-SeYFP constructs were developed and expression of fusion
413 viral proteins was analyzed in individually transfected or co-transfected cells by
414 fluorescence microscopy (Figure 4). We did not include any construct coding for a
415 fluorescently tagged SARS-CoV E protein because it does not tolerate fluorescent
416 protein tags (C. Chan et al., unpublished data). All chimeric viral proteins could be
417 readily observed by fluorescent microscopy. In cells individually transfected with
418 the pIRES-MmRFP1-E, the MmRFP1 fusion protein was mainly present in a
419 perinuclear compartment, most likely the ERGIC/Golgi apparatus (Figure 4, panels
420 a,b). We also found MmRFP1 within the cytoplasm and occasionally at the plasma
421 membrane. As expected, the SeYFP protein was observed both in the
422 ERGIC/Golgi apparatus, and at the plasma membrane of individually transfected
423 cells (Figure 4, panels c,d). These expression patterns are similar to what we
424 observed previously for MeGFP and SeGFP fusion proteins at 15 hours post-
425 infection with Semliki Forest Virus expression vectors (51). In most of the cells,
426 individually expressed NeCFP protein formed bright cytosolic patches, suggesting
427 aggregation of the protein in the cytosol in absence of functional viral protein
428 partners (Figure 4 e,f). This pattern may reflect large inclusions of nucleocapsids,

which have been described to accumulate late in the infection of cells with HCoV and MHV-JHM and SARS-CoV (6, 17, 23) or may constitute a cytosolic reservoir of protein supposed to feed the viral budding system. Interestingly, when plasmids were co-transfected, all three MmRFP1, SeYFP and NeCFP fluorescent proteins presented similar intracellular distributions, co-localizing in the cytoplasm and at the plasma membrane (Figure 4 panels g,i,k,m and h,j,l,n). When co-expressed with MmRFP1, E and SeYFP, the subcellular distribution of the NeCFP protein was dramatically changed and bright cytosolic patches were rarely found (Figure 4, panels e,f and k,l). Trafficking of NeCFP to the cell surface in co-transfected cells suggests that interactions with other viral proteins have occurred leading to NeCFP translocation. Nevertheless no VLPs were detected in medium from co-transfected cells (data not shown). Altogether, these results suggest that although MmRFP1, SeYFP, NeCFP and E are likely to interact when co-expressed in Vero E6 cells, they are not released in the form of VLPs in cell medium.

We then reasoned that fluorescent VLPs could be produced by including only one plasmid coding for one of the fluorescently tagged viral protein per co-transfection. In these conditions, we investigated protein expression and release of VLPs by Vero E6 cells at 48 hours post-transfection (Figure 5A). As positive control, we monitored VLP release from pIRES-M-E, pcDNA-Nflag, pcDNA-S transfected cells. As expected, S, Nflag, M and E proteins were detected in both cell lysate and VLP preparation (Figure 5A, lane 2 and 7). Although the MmRFP1 fusion protein was readily observed by fluorescent microscopy, it could not be detected by Western blot. Most likely, the rabbit polyclonal antibody directed against the M C-terminal domain cannot recognize its epitope when it is fused to the mRFP1 fluorescent tag. Although the E, Nflag and S proteins were detected on cell lysate

454 from pIRES-MmRFP1-E plus pcDNA-Nflag plus pcDNA-S transfected cells (Figure
455 5A, lane 3), no protein corresponding to purified VLPs were found in medium
456 (Figure 5A, lane 8). We concluded that fusion of the mRFP1 protein at the C-
457 terminal end of M inhibits VLP production. On the contrary, both pIRES-M-E plus
458 pcDNA-NeCFP plus pcDNA-S, as well as pIRES-M-E plus pcDNA-Nflag plus
459 pcDNA-SeYFP transfected cells were able to release VLPs in cell medium, as
460 indicated by the presence of viral proteins (figure 5A, lanes 9 and 10). Under these
461 conditions, the NeCFP protein was detected by a mouse monoclonal antibody
462 directed against N (56) and migrated to an apparent molecular size of 70 KDa.
463 To confirm that NeCFP or SeYFP viral proteins are correctly incorporated into
464 VLPs, we analyzed purified VLPs by fractionation on a 20-60% sucrose gradient
465 (Figure 5B). Both NeCFP and SeYFP co-sedimented with other viral proteins,
466 indicating that they were incorporated in purified VLPs (Figure 5B, upper and lower
467 panels, respectively). M-E-NeCFP-S VLPs were concentrated in fractions 10 and
468 11. The E protein was not detected, most likely because M-E-NeCFP-S VLPs
469 were less abundant in culture medium than M-E-Nflag-S VLPs for which E levels
470 were already low. M-E-Nflag-SeYFP VLPs were more efficiently produced and
471 concentrated in fractions 9 and 10 although high levels were also found in
472 fractions 6, 7 and 8. Considering the high levels of M and Nflag detected in these
473 fractions, incorporation of SeYFP seems less efficient than S (cf. Figure 2 with
474 Figure 5B, lower panel). Altogether, our results demonstrate that fluorescent VLPs
475 can be readily produced in Vero E6 transfected cells by incorporating either a
476 tagged N or S fusion protein.
477

Visualization of M-E-NeC/GFP-S VLP production and transport in living Vero E6 cells.

We then investigated formation and transport of fluorescent SARS-CoV VLPs in living transfected cells by fluorescent microscopy. Knowing that S is expressed all along the secretory pathway in both single- and co-transfected cells, we reasoned that N would be a better marker for monitoring of SARS-CoV VLPs assembly. Furthermore, having demonstrated that M, E and N are the crucial factors for assembly and egress of SARS-CoV VLPs, and anticipating that S-bearing VLPs could be internalized back into producer cells by ACE-2 driven endocytosis, we decided to omit S. Therefore, the pcDNA-NeCFP plasmid was either transfected alone or co-transfected with pIRES-M-E. Vero E6 cells were analyzed at 24 hours post-transfection. In most pcDNA-NeCFP transfected cells, eCFP signals were very bright and concentrated in large aggregates in the cytosol at the periphery of the nucleus (Figure 6A, panel a). Inversely and very interestingly, a different pattern was observed in most of cells co-transfected with pIRES-M-E and pcDNA-NeCFP. In these cells, eCFP fluorescence was more diffuse in cell cytosol: medium-size bright vesicles were concentrated in close proximity to the nucleus, smaller and dimmer vesicles were scattered in the cytoplasm and occasionally bright dots were enriched at the cell cortical area (Figure 6A, panels b). Few bright dots were also found outside cells in the surrounding medium. This difference in NeCFP distribution pattern, suggests that NeCFP assembles with co-expressed M and E viral proteins to form VLPs and traffics from the perinuclear assembly compartment to the cell surface where fluorescent VLPs are released into the medium.

We then further analyzed the trafficking dynamics of a fluorescently tagged N protein, co-expressed with M and E envelope proteins in living Vero E6 cells. In this aim, images were acquired using a spinning disc confocal microscope coupled to a CCD camera suitable for high-speed and high-resolution imaging. In these experiments we replaced the NeCFP by a NeGFP fusion protein, which is excitable by the Argon laser the microscope was equipped with. We could consistently identify three types of NeGFP containing vesicles, where fluorescent signal intensities, sizes and movements differ (Figure 6B and corresponding videos provided as supplementary data). First, the largest and brightest vesicles were found close to the nucleus and were static. Second, smaller and dimmer vesicles were trafficking actively, most of the time in a multidirectional way, making transient interactions with other vesicles. Occasionally these vesicles moved in rapid, unidirectional way and for longer distances, most likely along microtubules. Third, some cells presented an accumulation of bright dots at the cortical area, which may correspond to smaller secretory vesicles and released VLPs. Few bright dots were found outside cells, which probably correspond to fluorescent VLPs that have been released from producer cells. These results illustrate that fusion of a fluorescent tag to the C-terminal end of the nucleocapsid viral protein makes monitoring of SARS-CoV VLPs' egress possible.

We then investigated the effect of Brefeldin A (BFA), a fungal metabolite that has multiple effects upon the organelles of the secretory pathway, including inhibition of trafficking from ER to the Golgi apparatus, fusion of the cisternae of the Golgi with the ER and fusion of the trans-Golgi network (TGN) with endosomes (59). BFA has been used in previous study for analysis of viral protein transport and virus assembly (10, 49). Time-lapse images of living Vero E6 cells transfected with

M-E plus NeGFP were acquired at 24 hours post-transfection (Figure 6C; for video, see supplementary data). In a first time, cells were either non-treated (panel a) or treated with 6 μg / ml BFA for 4 hours (panel d) or over-night (panel g). After several minutes of acquisition in these conditions, medium was changed to either BFA-containing medium (panels b and c) or normal medium (panels e, f and h, i), respectively. New sequences of images were acquired and fluorescence redistribution was analyzed. Upon BFA treatment we observed fusion of scattered fluorescent vesicles into large cytosolic fluorescent clusters accumulating at the center of the cell and diminution of puncta (panels a, b and c, supplementary data). After treatment of cells for 4 hours with BFA, most of the fluorescence was present in large bright patches surrounding the nucleus (panel d). Vesicles could still be observed in the cytosol, although less numerous than in non-treated cells. Following BFA wash, we could not observe any obvious reversibility of the massive redistribution of fluorescence (compare panels d and e, panel f). After over-night incubation with BFA, fluorescence was associated with large cytosolic clusters and endoplasmic reticulum (panel g) and no drastic change was observed after BFA wash and 1:30 hours recovery (panel h), although membrane dynamics seem to increase at the edge on the reticular compartment where tubules elongated from (panel h, arrow; supplementary data). Three hours recovery after over-night BFA treatment partially restore trafficking of fluorescent vesicles in transfected cells (panel i). The recovery process after BFA treatment was slow and the dynamics could not be followed for several hours, as repetitive exposure to laser induced apoptosis. Altogether, our results suggest 1/ that BFA induce reorganization of NeGFP associated compartments and alters vesicle formation and transport, 2/ that several hours of recovery after BFA wash are necessary to

552 restore dynamics of NeGFP associated compartment and vesicles trafficking.
553 Further studies are required in order to clarify the subcellular compartments VLPs
554 are associated with and delineate the dynamics of egress in association with
555 cellular structures.
556

Discussion

The minimal molecular requirement for efficient assembly and egress of SARS-CoV virions is still controversial. Here we describe the development of a plasmid-based transfection method for efficient production and release of SARS-CoV VLPs in permissive Vero E6 green monkey kidney epithelial cells. In contrast to reports on other coronaviruses, we demonstrate that all three M, E and N SARS-CoV structural proteins are required for efficient assembly and release of VLPs by transfected cells. When the S viral envelope glycoprotein is co-expressed with M, N and E, trimers of S are incorporated onto VLPs. Of particular interest is the finding that incorporation of a fluorescently tagged N protein into VLPs allows visualization of transport of *de-novo* formed particles in producer cells. Fluorescent VLPs constitute a new powerful model to study the mechanisms of SARS-CoV egress in living cells and specific roles of cellular machineries by fluorescence imaging techniques.

Other research groups have described formation of SARS-CoV VLPs in either insect (26, 44, 50) or mammalian cells (27-29), using various expression systems. Huang Y. and colleagues were the first to report generation of SARS-CoV VLPs in human 293 renal epithelial cells (29). Human codon optimized genes encoding for M, E, N and S proteins were subcloned into mammalian expression vector and VLP formation was monitored by transmission electron microscopy on transfected cells at 63 hours post-transfection. The authors show that, in their experimental conditions, M and N are necessary and sufficient for formation of intracellular VLPs, independently of E and S, but secretion of VLPs was not efficient. Moreover, they described S as an important viral factor for maturation and egress

582 of VLPs from cells, but release of M-N-S VLPs in culture medium was still
583 inefficient. By contrast, in our system we detected sedimentable M and N proteins
584 in culture medium from M plus N expressing cells, suggesting that M-N VLPs can
585 form and be secreted (Figure 1). Furthermore, co-expression of E greatly boosted
586 levels of VLPs detected in culture medium (Figure 1) and addition of S did not
587 influence the rate of VLP production (Figure 2 and data not shown). In contrast,
588 Hsieh and colleagues have described that co-expressed E and M proteins are
589 released four days post-transfection in culture medium of Vero E6 cells in the
590 absence of S and N proteins. In their study, Vero E6 cells, previously infected with
591 a recombinant vaccinia virus harboring the T7 polymerase gene, were co-
592 transfected with plasmids encoding MycHis or V5His-tagged S, M, E and N
593 structural proteins. Nevertheless, sedimentable E and M proteins were also found
594 in culture medium even when they were individually expressed and very high
595 amounts of E were found in VLP preparations in comparison to other viral proteins,
596 suggesting formation of E-containing vesicles. Others have described that MHV
597 and IBV E protein expressed alone results in assembly of E-protein-containing
598 vesicles, with a density similar to that of VLPs (7, 47). We too did find
599 sedimentable SARS-CoV E proteins in culture medium from individually pcDNA-E
600 transfected cells, suggesting secretion of E vesicles, but we could not detect them
601 in any fraction after sucrose gradient fractionation, suggesting a low production
602 rate (Figure 1). We could also detect M-E VLPs at 48 hours post-transfection by
603 coexpressing both E and M proteins, albeit at very low levels (Figure 1A, B and C).
604 In our study, we took advantage of the pIRES bicistronic vector to ensure
605 concomitant expression of E and M and maintain a low expression level for E. We
606 show that use of this vector system, in combination with expression of N, ensures

607 slightly better levels of M-E-N VLPs in medium and great incorporation of E
608 (Figure 1B). Higher levels of E were expressed when an individual pcDNA-E
609 vector was used for E expression and resulted in increased E/M and E/N ratio in
610 cell medium (Figure 1B). We could not conclude whether this was due to higher
611 level of E incorporation into VLPs or to simultaneous release of E-containing
612 vesicles and VLPs. Analysis of viral protein in cell medium by sucrose gradient
613 fractionation revealed that E was only released at significant levels when co-
614 expressed with M and N proteins, with which it cosediments (Figure 1C, panels b,
615 c and e). We have observed efficient M-E-N-S VLP formation and release in 293T,
616 HeLa and Huh-7 human cell lines (data not shown). Consistently, formation and
617 release of M-E-N-S VLPs from 293T cells has been shown in another study
618 reported by Huang C. and colleagues, in which authors have used a pCAGGS
619 mammalian expression plasmid-based transfection system (28). Huang C. and
620 colleagues were able to generate approximately 1.3 μg of SARS-CoV VLPs from
621 2.10^7 293T cells (42). Recently, we have measured quantity of S incorporated into
622 envelope of M-E-N-S VLPs purified from the VLP-containing sucrose fractions in
623 our system. Approximately 1μg and 28 μg of S were present in VLP preparations
624 from 10^7 VeroE6 and 293T cells, respectively (data not shown).
625 We also investigated formation and secretion of SARS-CoV VLPs in transfected
626 cells by transmission electron microscopy and negative staining of purified
627 secreted particles (Figure 3). We were able to identify budding events in
628 cytoplasmic perinuclear compartments. VLP-containing vesicles were scattered
629 within the cytoplasm and found beneath the plasma membrane. Occasionally,
630 secreted VLPs were bound to the cell surface. The VLPs-associated
631 compartments that we observed in transfected Vero E6 cells share significant

632 similarities with the virions-containing compartments described in SARS-CoV
633 infected Vero E6 cells at 3-5 days post infection (23). VLPs were readily detected
634 in sedimented fractions from culture medium by negative staining and electron
635 microscopy (Figure 3H). Globular structures protruding from VLP envelope, and
636 which should correspond to spike peplomers, were occasionally detected, but we
637 could not identify any particle displaying a typical corona-like structure attesting for
638 optimal incorporation of spike trimers on virion envelope.
639 Interestingly, we found that a C-terminal Flag or eYFP tag affects levels of S
640 trimers incorporation onto VLPs (data not shown and Figure 5, respectively).
641 However Sflag and SeYFP proteins could still be incorporated into VLPs and tags
642 can be used as markers. Similar results had been obtained for MHV where S
643 sequence had been extended by fusion with a GFP fluorescent protein (3). These
644 data can be explained by several factors: the 30 KDa fluorescent protein may
645 cause geometrical constraints; M-S interactions, which are important for S
646 incorporation may be affected by the tag; S retention to the site of viral assembly
647 may be disturbed (43, 48). We also tried to produce VLPs containing the mRFP1
648 fluorescent protein fused to the C-terminal end of M (Figure 4 and 5A). Although
649 MmRFP1 was expressed in transfected cells, production of VLPs was abrogated.
650 The M endodomain is crucial for M-N, M-E and M-S interactions and VLP
651 formation (8, 11, 13, 19) and its fusion to a fluorescent protein tag may affect its
652 structure and/or availability for interaction with other partners. This hypothesis is
653 reinforced by the complete loss of recognition of the chimeric MmRFP1 by a rabbit
654 serum raised against a C-terminal peptide of M (Figure 5A, left panel).
655 Lastly, a fusion NeCFP protein could be expressed and assemble into VLPs with
656 M, E and S, although levels of VLPs detected in culture medium were significantly

reduced (Figure 5). Interestingly, whereas individually expressed NeCFP or NeGFP were found in the cell cytosol, often accumulating in the perinuclear area, the tagged N protein had a tendency to display a vesicular distribution pattern when co-expressed with M and E (Figure 6). We analyzed both distribution and trafficking of the NeGFP protein in transfected live cells by confocal microscopy (Figure 6B). When cells were co-transfected with pIRES-M-E and pcDNA-NeGFP, the NeGFP proteins were often found in static compartment near the nucleus, in trafficking vesicles scattered in the cytosol and moving actively, making transient interactions with other vesicles, and as small dot scattered at the cortical area beneath the plasma membrane, often enriched in cell projections. Fluorescent dots were also detected in the cell medium surrounding living cells. Subcellular distribution of NeGFP is consistent with our data of transmission electron microscopy. Most likely perinuclear static compartments and trafficking vesicles identified by fluorescence microscopy correspond to perinuclear vacuoles, at which membranes VLP budding events were observed, and to VLP-containing vesicles found by electron microscopy, respectively. The fluorescent dots observed at the cell cortical area may correspond to smaller secretory vesicles containing fewer VLPs – vesicles containing only one VLP were found by electron microscopy – and/or to released VLPs, which are bound to the cell surface. Interestingly, transport of fluorescent vesicles was affected by the drug BFA, well known to affect membrane transport in the secretory pathway (39, 59). BFA treatment induced backward trafficking of fluorescent vesicles and fusion into bright perinuclear clusters (Figure 6C panels a, b and c). Long lasting BFA treatment resulted in suppression of vesicle trafficking and no fluorescent puncta

681 were found at plasma membrane (Figure 6C panel g) and recovery of vesicle
682 trafficking was restored after several hours in normal medium (Figure 6C panel i).
683 Altogether, our data demonstrate that M, E and N structural proteins are key
684 molecules for assembly and egress of the SARS-CoV. Production and analysis of
685 fluorescent M-E-NeGFP SARS-CoV VLPs in living cells allowed us to identify
686 three subcellular structures with different velocity characteristics along the
687 secretory pathway. Molecular and cellular determinants of SARS-CoV assembly
688 and egress will be investigated further using advanced fluorescence microscopy
689 techniques.

690 **Acknowledgements**

691

692 We would like to thank Dr KH Chan (Department of Microbiology, University of
693 Hong Kong) for the gift of the mouse monoclonal antibody against the SARS-CoV
694 N protein, and Professor Roger Y Tsien (University of California, San Diego) for
695 providing us with the plasmid coding for the mRFP1 protein. Special thanks to the
696 Electron microscope Unit of The University of Hong Kong, Li Ka Shing Faculty of
697 Medicine, to Mme Marie-Christine Prevost and Dr Martin Sachse (Plate-Forme de
698 Microscopie Electronique, Institut Pasteur) for their expert advices on electron
699 microscopy experiments; to Ms Iris Ng (Department of Microbiology, University of
700 Hong Kong) for her technical support for electron microscopy experiments; and to
701 Mr Tony Chan (Department of Anatomy, Li Ka Shing Faculty of Medicine Core
702 Imaging Facility, University of Hong Kong) for his technical support during the live
703 cell imaging experiments. KTT is a PhD student supported by the University of
704 Hong Kong. This work was supported by the French Ministry of Health (through
705 the RESPARI Program of the International Network of Institut Pasteur), the French
706 Chancery of Paris Universities and the EU-6th Framework Program (EPISARS).

References

1. **Baudoux, P., C. Carrat, L. Besnardeau, B. Charley, and H. Laude.** 1998. Coronavirus pseudoparticles formed with recombinant M and E proteins induce alpha interferon synthesis by leukocytes. J Virol **72:**8636-43.

2. **Bos, E. C., W. Luytjes, H. V. van der Meulen, H. K. Koerten, and W. J. Spaan.** 1996. The production of recombinant infectious DI-particles of a murine coronavirus in the absence of helper virus. Virology **218:**52-60.

3. **Bosch, B. J., C. A. de Haan, and P. J. Rottier.** 2004. Coronavirus spike glycoprotein, extended at the carboxy terminus with green fluorescent protein, is assembly competent. J Virol **78:**7369-78.

4. **Bosch, B. J., C. A. de Haan, S. L. Smits, and P. J. Rottier.** 2005. Spike protein assembly into the coronavirion: exploring the limits of its sequence requirements. Virology **334:**306-18.

5. **Campbell, R. E., O. Tour, A. E. Palmer, P. A. Steinbach, G. S. Baird, D. A. Zacharias, and R. Y. Tsien.** 2002. A monomeric red fluorescent protein. Proc Natl Acad Sci U S A **99:**7877-82.

6. **Caul, E. O., and S. I. Egglestone.** 1977. Further studies on human enteric coronaviruses. Arch Virol **54:**107-17.

7. **Corse, E., and C. E. Machamer.** 2000. Infectious bronchitis virus E protein is targeted to the Golgi complex and directs release of virus-like particles. J Virol **74:**4319-26.

8. **Corse, E., and C. E. Machamer.** 2003. The cytoplasmic tails of infectious bronchitis virus E and M proteins mediate their interaction. Virology **312:**25-34.

9. **Curtis, K. M., B. Yount, and R. S. Baric.** 2002. Heterologous gene expression from transmissible gastroenteritis virus replicon particles. J Virol **76:**1422-34.

10. **Dasgupta, A., and D. W. Wilson.** 2001. Evaluation of the primary effect of brefeldin A treatment upon herpes simplex virus assembly. J Gen Virol **82:**1561-7.

11. **de Haan, C. A., L. Kuo, P. S. Masters, H. Vennema, and P. J. Rottier.** 1998. Coronavirus particle assembly: primary structure requirements of the membrane protein. J Virol **72:**6838-50.

12. **de Haan, C. A., and P. J. Rottier.** 2005. Molecular interactions in the assembly of coronaviruses. Adv Virus Res **64:**165-230.

13. **de Haan, C. A., M. Smeets, F. Vernooij, H. Vennema, and P. J. Rottier.** 1999. Mapping of the coronavirus membrane protein domains involved in interaction with the spike protein. J Virol **73:**7441-52.

14. **de Haan, C. A., H. Vennema, and P. J. Rottier.** 2000. Assembly of the coronavirus envelope: homotypic interactions between the M proteins. J Virol **74:**4967-78.

15. **Decaro, N., V. Mari, C. Desario, M. Campolo, G. Elia, V. Martella, G. Greco, F. Cirone, M. L. Colaianni, P. Cordioli, and C. Buonavoglia.** 2008. Severe outbreak of bovine coronavirus infection in dairy cattle during the warmer season. Vet Microbiol **126:**30-9.

16. **DeDiego, M. L., E. Alvarez, F. Almazan, M. T. Rejas, E. Lamirande, A. Roberts, W. J. Shieh, S. R. Zaki, K. Subbarao, and L. Enjuanes.** 2007. A severe acute respiratory syndrome coronavirus that lacks the E gene is attenuated in vitro and in vivo. J Virol **81:**1701-13.

17. **Dubois-Dalcq, M. E., E. W. Doller, M. V. Haspel, and K. V. Holmes.** 1982. Cell tropism and expression of mouse hepatitis viruses (MHV) in mouse spinal cord cultures. Virology **119:**317-31.

18. **Erles, K., C. Toomey, H. W. Brooks, and J. Brownlie.** 2003. Detection of a group 2 coronavirus in dogs with canine infectious respiratory disease. Virology **310:**216-23.

19. **Escors, D., J. Ortego, H. Laude, and L. Enjuanes.** 2001. The membrane M protein carboxy terminus binds to transmissible gastroenteritis coronavirus core and contributes to core stability. J Virol **75:**1312-24.

20. **Fischer, F., C. F. Stegen, P. S. Masters, and W. A. Samsonoff.** 1998. Analysis of constructed E gene mutants of mouse hepatitis virus confirms a pivotal role for E protein in coronavirus assembly. J Virol **72:**7885-94.

21. **Fouchier, R. A., T. Kuiken, M. Schutten, G. van Amerongen, G. J. van Doornum, B. G. van den Hoogen, M. Peiris, W. Lim, K. Stohr, and A. D. Osterhaus.** 2003. Aetiology: Koch's postulates fulfilled for SARS virus. Nature **423:**240.

22. **Godet, M., R. L'Haridon, J. F. Vautherot, and H. Laude.** 1992. TGEV corona virus ORF4 encodes a membrane protein that is incorporated into virions. Virology **188:**666-75.

23. **Goldsmith, C. S., K. M. Tatti, T. G. Ksiazek, P. E. Rollin, J. A. Comer, W. W. Lee, P. A. Rota, B. Bankamp, W. J. Bellini, and S. R. Zaki.** 2004. Ultrastructural characterization of SARS coronavirus. Emerg Infect Dis **10:**320-6.

24. **He, R., F. Dobie, M. Ballantine, A. Leeson, Y. Li, N. Bastien, T. Cutts, A. Andonov, J. Cao, T. F. Booth, F. A. Plummer, S. Tyler, L. Baker, and X. Li.**

779 2004. Analysis of multimerization of the SARS coronavirus nucleocapsid protein.
780 Biochem Biophys Res Commun **316:**476-83.
781 25. **He, R., A. Leeson, M. Ballantine, A. Andonov, L. Baker, F. Dobie, Y. Li,**
782 **N. Bastien, H. Feldmann, U. Strocher, S. Theriault, T. Cutts, J. Cao, T. F.**
783 **Booth, F. A. Plummer, S. Tyler, and X. Li.** 2004. Characterization of protein-
784 protein interactions between the nucleocapsid protein and membrane protein of
785 the SARS coronavirus. Virus Res **105:**121-5.
786 26. **Ho, Y., P. H. Lin, C. Y. Liu, S. P. Lee, and Y. C. Chao.** 2004. Assembly of
787 human severe acute respiratory syndrome coronavirus-like particles. Biochem
788 Biophys Res Commun **318:**833-8.
789 27. **Hsieh, P. K., S. C. Chang, C. C. Huang, T. T. Lee, C. W. Hsiao, Y. H.**
790 **Kou, I. Y. Chen, C. K. Chang, T. H. Huang, and M. F. Chang.** 2005. Assembly of
791 severe acute respiratory syndrome coronavirus RNA packaging signal into virus-
792 like particles is nucleocapsid dependent. J Virol **79:**13848-55.
793 28. **Huang, C., N. Ito, C. T. Tseng, and S. Makino.** 2006. Severe acute
794 respiratory syndrome coronavirus 7a accessory protein is a viral structural protein.
795 J Virol **80:**7287-94.
796 29. **Huang, Y., Z. Y. Yang, W. P. Kong, and G. J. Nabel.** 2004. Generation of
797 synthetic severe acute respiratory syndrome coronavirus pseudoparticles:
798 implications for assembly and vaccine production. J Virol **78:**12557-65.
799 30. **Hurst, K. R., L. Kuo, C. A. Koetzner, R. Ye, B. Hsue, and P. S. Masters.**
800 2005. A major determinant for membrane protein interaction localizes to the
801 carboxy-terminal domain of the mouse coronavirus nucleocapsid protein. J Virol
802 **79:**13285-97.

803 31. **Kam, Y. W., F. Kien, A. Roberts, Y. C. Cheung, E. W. Lamirande, L.**
804 **Vogel, S. L. Chu, J. Tse, J. Guarner, S. Zaki, K. Subbarao, M. Peiris, B. Nal,**
805 **and R. Altmeyer.** 2006. Antibodies against trimeric S glycoprotein protect
806 hamsters against SARS-CoV challenge despite their capacity to mediate
807 FcgammaRII-dependent entry into B cells in vitro. Vaccine.
808 32. **Klumperman, J., J. K. Locker, A. Meijer, M. C. Horzinek, H. J. Geuze,**
809 **and P. J. Rottier.** 1994. Coronavirus M proteins accumulate in the Golgi complex
810 beyond the site of virion budding. J Virol **68:**6523-34.
811 33. **Krijnse-Locker, J., M. Ericsson, P. J. Rottier, and G. Griffiths.** 1994.
812 Characterization of the budding compartment of mouse hepatitis virus: evidence
813 that transport from the RER to the Golgi complex requires only one vesicular
814 transport step. J Cell Biol **124:**55-70.
815 34. **Ksiazek, T. G., D. Erdman, C. S. Goldsmith, S. R. Zaki, T. Peret, S.**
816 **Emery, S. Tong, C. Urbani, J. A. Comer, W. Lim, P. E. Rollin, S. F. Dowell, A.**
817 **E. Ling, C. D. Humphrey, W. J. Shieh, J. Guarner, C. D. Paddock, P. Rota, B.**
818 **Fields, J. DeRisi, J. Y. Yang, N. Cox, J. M. Hughes, J. W. LeDuc, W. J. Bellini,**
819 **and L. J. Anderson.** 2003. A novel coronavirus associated with severe acute
820 respiratory syndrome. N Engl J Med **348:**1953-66.
821 35. **Kuo, L., K. R. Hurst, and P. S. Masters.** 2007. Exceptional flexibility in the
822 sequence requirements for coronavirus small envelope protein function. J Virol
823 **81:**2249-62.
824 36. **Kuo, L., and P. S. Masters.** 2002. Genetic evidence for a structural
825 interaction between the carboxy termini of the membrane and nucleocapsid
826 proteins of mouse hepatitis virus. J Virol **76:**4987-99.

827 37. **Kuo, L., and P. S. Masters.** 2003. The small envelope protein E is not
828 essential for murine coronavirus replication. J Virol **77:**4597-608.
829 38. **Lim, K. P., and D. X. Liu.** 2001. The missing link in coronavirus assembly.
830 Retention of the avian coronavirus infectious bronchitis virus envelope protein in
831 the pre-Golgi compartments and physical interaction between the envelope and
832 membrane proteins. J Biol Chem **276:**17515-23.
833 39. **Lippincott-Schwartz, J., L. C. Yuan, J. S. Bonifacino, and R. D.**
834 **Klausner.** 1989. Rapid redistribution of Golgi proteins into the ER in cells treated
835 with brefeldin A: evidence for membrane cycling from Golgi to ER. Cell **56:**801-13.
836 40. **Liu, D. X., and S. C. Inglis.** 1991. Association of the infectious bronchitis
837 virus 3c protein with the virion envelope. Virology **185:**911-7.
838 41. **Locker, J. K., D. J. Opstelten, M. Ericsson, M. C. Horzinek, and P. J.**
839 **Rottier.** 1995. Oligomerization of a trans-Golgi/trans-Golgi network retained
840 protein occurs in the Golgi complex and may be part of its retention. J Biol Chem
841 **270:**8815-21.
842 42. **Lokugamage, K. G., N. Yoshikawa-Iwata, N. Ito, D. M. Watts, P. R.**
843 **Wyde, N. Wang, P. Newman, C. T. Kent Tseng, C. J. Peters, and S. Makino.**
844 2008. Chimeric coronavirus-like particles carrying severe acute respiratory
845 syndrome coronavirus (SCoV) S protein protect mice against challenge with
846 SCoV. Vaccine **26:**797-808.
847 43. **Lontok, E., E. Corse, and C. E. Machamer.** 2004. Intracellular Targeting
848 Signals Contribute to Localization of Coronavirus Spike Proteins near the Virus
849 Assembly Site. J Virol **78:**5913-22.
850 44. **Lu, X., Y. Chen, B. Bai, H. Hu, L. Tao, J. Yang, J. Chen, Z. Chen, Z. Hu,**
851 **and H. Wang.** 2007. Immune responses against severe acute respiratory

852 syndrome coronavirus induced by virus-like particles in mice. Immunology
853 **122:**496-502.
854 45. **Luo, H., D. Wu, C. Shen, K. Chen, X. Shen, and H. Jiang.** 2006. Severe
855 acute respiratory syndrome coronavirus membrane protein interacts with
856 nucleocapsid protein mostly through their carboxyl termini by electrostatic
857 attraction. Int J Biochem Cell Biol **38:**589-99.
858 46. **Madan, V., J. Garcia Mde, M. A. Sanz, and L. Carrasco.** 2005. Viroporin
859 activity of murine hepatitis virus E protein. FEBS Lett **579:**3607-12.
860 47. **Maeda, J., A. Maeda, and S. Makino.** 1999. Release of coronavirus E
861 protein in membrane vesicles from virus-infected cells and E protein-expressing
862 cells. Virology **263:**265-72.
863 48. **McBride, C. E., J. Li, and C. E. Machamer.** 2007. The cytoplasmic tail of
864 the severe acute respiratory syndrome coronavirus spike protein contains a novel
865 endoplasmic reticulum retrieval signal that binds COPI and promotes interaction
866 with membrane protein. J Virol **81:**2418-28.
867 49. **Mirazimi, A., C. H. von Bonsdorff, and L. Svensson.** 1996. Effect of
868 brefeldin A on rotavirus assembly and oligosaccharide processing. Virology
869 **217:**554-63.
870 50. **Mortola, E., and P. Roy.** 2004. Efficient assembly and release of SARS
871 coronavirus-like particles by a heterologous expression system. FEBS Lett
872 **576:**174-8.
873 51. **Nal, B., C. Chan, F. Kien, L. Siu, J. Tse, K. Chu, J. Kam, I. Staropoli, B.
874 Crescenzo-Chaigne, N. Escriou, S. van der Werf, K. Y. Yuen, and R.
875 Altmeyer.** 2005. Differential maturation and subcellular localization of severe

876 acute respiratory syndrome coronavirus surface proteins S, M and E. J Gen Virol
877 **86:**1423-34.
878 52. **Narayanan, K., K. H. Kim, and S. Makino.** 2003. Characterization of N
879 protein self-association in coronavirus ribonucleoprotein complexes. Virus Res
880 **98:**131-40.
881 53. **Narayanan, K., A. Maeda, J. Maeda, and S. Makino.** 2000.
882 Characterization of the coronavirus M protein and nucleocapsid interaction in
883 infected cells. J Virol **74:**8127-34.
884 54. **Narayanan, K., and S. Makino.** 2001. Characterization of nucleocapsid-M
885 protein interaction in murine coronavirus. Adv Exp Med Biol **494:**577-82.
886 55. **Nguyen, V. P., and B. G. Hogue.** 1997. Protein interactions during
887 coronavirus assembly. J Virol **71:**9278-84.
888 56. **Nicholls, J. M., J. Butany, L. L. Poon, K. H. Chan, S. L. Beh, S.**
889 **Poutanen, J. S. Peiris, and M. Wong.** 2006. Time course and cellular localization
890 of SARS-CoV nucleoprotein and RNA in lungs from fatal cases of SARS. PLoS
891 Med **3:**e27.
892 57. **Ortego, J., D. Escors, H. Laude, and L. Enjuanes.** 2002. Generation of a
893 replication-competent, propagation-deficient virus vector based on the
894 transmissible gastroenteritis coronavirus genome. J Virol **76:**11518-29.
895 58. **Peiris, J. S., S. T. Lai, L. L. Poon, Y. Guan, L. Y. Yam, W. Lim, J.**
896 **Nicholls, W. K. Yee, W. W. Yan, M. T. Cheung, V. C. Cheng, K. H. Chan, D. N.**
897 **Tsang, R. W. Yung, T. K. Ng, and K. Y. Yuen.** 2003. Coronavirus as a possible
898 cause of severe acute respiratory syndrome. Lancet **361:**1319-25.
899 59. **Pelham, H. R.** 1991. Multiple targets for brefeldin A. Cell **67:**449-51.

60. **Rota, P. A., M. S. Oberste, S. S. Monroe, W. A. Nix, R. Campagnoli, J. P. Icenogle, S. Penaranda, B. Bankamp, K. Maher, M. H. Chen, S. Tong, A. Tamin, L. Lowe, M. Frace, J. L. DeRisi, Q. Chen, D. Wang, D. D. Erdman, T. C. Peret, C. Burns, T. G. Ksiazek, P. E. Rollin, A. Sanchez, S. Liffick, B. Holloway, J. Limor, K. McCaustland, M. Olsen-Rasmussen, R. Fouchier, S. Gunther, A. D. Osterhaus, C. Drosten, M. A. Pallansch, L. J. Anderson, and W. J. Bellini.** 2003. Characterization of a novel coronavirus associated with severe acute respiratory syndrome. Science **300:**1394-9.

61. **Schelle, B., N. Karl, B. Ludewig, S. G. Siddell, and V. Thiel.** 2006. Nucleocapsid protein expression facilitates coronavirus replication. Adv Exp Med Biol **581:**43-8.

62. **Stertz, S., M. Reichelt, M. Spiegel, T. Kuri, L. Martinez-Sobrido, A. Garcia-Sastre, F. Weber, and G. Kochs.** 2007. The intracellular sites of early replication and budding of SARS-coronavirus. Virology **361:**304-15.

63. **Tooze, J., S. Tooze, and G. Warren.** 1984. Replication of coronavirus MHV-A59 in sac- cells: determination of the first site of budding of progeny virions. Eur J Cell Biol **33:**281-93.

64. **van der Hoek, L., K. Pyrc, M. F. Jebbink, W. Vermeulen-Oost, R. J. Berkhout, K. C. Wolthers, P. M. Wertheim-van Dillen, J. Kaandorp, J. Spaargaren, and B. Berkhout.** 2004. Identification of a new human coronavirus. Nat Med **10:**368-73.

65. **Vennema, H., G. J. Godeke, J. W. Rossen, W. F. Voorhout, M. C. Horzinek, D. J. Opstelten, and P. J. Rottier.** 1996. Nucleocapsid-independent assembly of coronavirus-like particles by co-expression of viral envelope protein genes. Embo J **15:**2020-8.

66. **Wilson, L., P. Gage, and G. Ewart.** 2006. Hexamethylene amiloride blocks E protein ion channels and inhibits coronavirus replication. Virology **353:**294-306.

67. **Wilson, L., C. McKinlay, P. Gage, and G. Ewart.** 2004. SARS coronavirus E protein forms cation-selective ion channels. Virology **330:**322-31.

68. **Woo, P. C., S. K. Lau, C. M. Chu, K. H. Chan, H. W. Tsoi, Y. Huang, B. H. Wong, R. W. Poon, J. J. Cai, W. K. Luk, L. L. Poon, S. S. Wong, Y. Guan, J. S. Peiris, and K. Y. Yuen.** 2005. Characterization and complete genome sequence of a novel coronavirus, coronavirus HKU1, from patients with pneumonia. J Virol **79:**884-95.

69. **Woo, P. C., S. K. Lau, K. S. Li, R. W. Poon, B. H. Wong, H. W. Tsoi, B. C. Yip, Y. Huang, K. H. Chan, and K. Y. Yuen.** 2006. Molecular diversity of coronaviruses in bats. Virology **351:**180-7.

70. **Ye, Y., and B. G. Hogue.** 2007. Role of the coronavirus E viroporin protein transmembrane domain in virus assembly. J Virol **81:**3597-607.

940 **Figure legends**

941

942 **Figure 1. Production of SARS-CoV VLPs by transfected Vero E6 cells. A.**
943 Coexpression of M, E and N is necessary for efficient secretion of SARS-CoV
944 VLPs by Vero E6 cells at 24 and 48 hours post-transfection. Monolayers of Vero
945 E6 cells were transfected with plasmids driving the expression of SARS-CoV
946 structural proteins M, E and Flag-tagged N as specified on top of each lane.
947 Protein expression in cell lysates and in VLPs isolated from culture medium was
948 analyzed by Western blot at 24 and 48 hours post-transfection, as indicated below
949 corresponding panels. Samples were heat-denatured and reduced with
950 dithiothreitol before loading. The M and E proteins were detected with rabbit
951 polyclonal antibodies produced against the C-terminal extremity of each proteins.
952 The N protein was detected with the M2 monoclonal antibody recognizing the Flag
953 tag. Blots were exposed for 1 minute for signal detection except for detection of E
954 contained in pellets from ultracentrifuged culture medium (bottom panels), for
955 which blots were exposed for 10 minutes. The molecular mass (in kDa) and
956 migration of protein standards are shown between blots. **B.** Use of the bicistronic
957 pIRES-M-E vector restrains E expression level and favors production of M-E-N
958 VLPs. Vero E6 were transfected with indicated plasmid combinations and cell
959 lysates and medium were analyzed at 48 hours post-transfection as in A. To
960 ensure better detection of E, VLPs were concentrated four times more than in A.
961 Blots were exposed for 10 seconds for signal detection except for detection of E
962 contained in pellets from ultracentrifuged culture medium (right bottom panel) for
963 which the blot was exposed for 1 minute. **C.** Secreted viral structural proteins
964 cosediment in sucrose gradient. Three 75 cm^2 dishes of Vero E6 cells were

965 transfected with plasmids driving the expression of SARS-CoV structural proteins
966 M, E and Flag-tagged N either individually or in combination. Protein expression in
967 cell lysates and in pellets from culture medium ultracentrifuged on 20% sucrose
968 cushion was controlled by Western blot at 48 hours post-transfection (left panel).
969 Resuspended pellets from ultracentrifuged cell medium were then loaded on a 20-
970 60% discontinuous sucrose gradient and subjected to fractionation by
971 ultracentrifugation. Twenty fractions of 600 μl were collected (1-20, lightest to
972 heaviest). Nature of viral proteins associated with each fraction was determined by
973 Western blot (right panels, a to e). 15 μl of samples were heat-denatured and
974 reduced with dithiothreitol before loading. The molecular mass (in kDa) and
975 migration of protein standards are shown on the right side of the blots. Samples
976 from pIRES-M, pIRES-E plus pCDNA-E, pIRES-E plus pCDNA-E pluspcDNA-
977 Nflag and pcDNA-E, pIRES-M plus pcDNA-Nflag have been generated in two
978 separate experiments.
979 Ctrl: non-transfected cells; E: pCDNA-E; M: pIRES-M; M-E: pIRES-M-E; M +
980 Nflag: pIRES-M plus pcDNA-Nflag; M-E + Nflag: pIRES-M-E plus pcDNA-Nflag; M
981 + E: pIRES-M + pcDNA-E; M + E + Nflag: pIRES-M plus pcDNA-E plus pcDNA-
982 Nflag.
983
984 **Figure 2. S glycoprotein trimers are incorporated onto SARS-CoV M, E and**
985 **N-containing VLPs.** pcDNA-S plasmid was co-transfected with pIRES-M-E and
986 pcDNA-Nflag vectors. Culture medium was harvested at 48 hours post-
987 transfection, ultracentrifuged on 20% sucrose cushion and pellets were
988 resuspended in TNE buffer and ultracentrifuged on a 20-60% discontinuous
989 sucrose gradient. Twenty fractions were collected (1-20, lightest to heaviest) and

990 analyzed by Western blot. Samples were either heat-denatured and reduced with
991 dithiothreitol before loading for detection of Nflag, M and E or not heated and not
992 reduced for analysis of S. Blots were exposed for 10 seconds for signal detection,
993 except for E for which blots were exposed for 10 minutes. The highest levels of S,
994 M, N and E structural proteins were found in fractions 9 and 10 corresponding to
995 40% sucrose. S protein was detected with mouse polyclonal antibodies raised
996 against purified S trimers. Arrows indicate bands that correspond to trimeric and
997 monomeric forms of S. The molecular mass (in kDa) and migration of protein
998 standards are shown on the right side of the blots.
999
1000 **Figure 3. Structural analysis and intracellular distribution of SARS-CoV**
1001 **VLPs.** Vero E6 cells were co-transfected with pIRES-M-E, pcDNA-Nflag and
1002 pcDNA-S. At 24 and 48 hours post-transfection cells were fixed and ultrathin
1003 sections were analyzed by electron microscopy (panels A to G). **A.** VLPs were
1004 found in intracellular vacuoles (vc), in vesicles (vs) scattered in the cytosol and
1005 bound to the plasma membrane (pm). The arrow points VLPs attached to the cell
1006 surface. **B.** Large amount of VLPs within the lumen of the endoplasmic reticulum
1007 (er) and within a cytoplasmic vesicle. n: nucleus. **C.** Presence of VLPs within
1008 vacuoles and vesicles. Arrows point to small VLPs-containing vesicles beneath the
1009 plasma membrane. **D.** Magnification of a VLP-containing vacuole. Black arrows
1010 point to budding events. **E.** Compacted VLP-containing vesicles were found
1011 beneath the plasma membrane. **F.** VLPs bound to the surface of a producer cell.
1012 Two membrane-bound VLPs are shown by arrows. **G.** VLPs bound to a cell
1013 filopodia. Spike-like protuberances were visible on VLP surface (arrows). **H.**
1014 Electron microscopy images of negatively stained VLPs purified from cell medium

at 48 hours post-transfection. A scale bar is indicated for each picture. A-D and F-G panels correspond to cells fixed at 48 hours post-transfection. Image E was taken from cells fixed 24 hours post-transfection. n: nucleus, er: endoplasmic reticulum, vc: vacuole, vs: vesicle, pm: plasma membrane.

Figure 4. Expression and subcellular distribution of viral structural proteins tagged with fluorescent proteins. Vero E6 cells grown on glass coverslips were either transfected with single plasmids (left panels) or co-transfected (right panels) with the three plasmids encoding the MmRFP1, E, SeYFP and NeCFP proteins. At 24 hours post-transfection, cells were processed for nuclear staining with DAPI dye, fixed and analyzed under a fluorescent microscope equipped with an ApoTome device to acquire images of optical sections. a, b, g, h: MmRFP1; c, d, I, j: SeYFP; e, f, k, l: NeCFP; m, n: merged images. For all conditions, two representative images are shown side-by-side.

Figure 5. Production of fluorescent VLPs by transfected Vero E6 cells. A. Determination of optimal plasmid combinations for production of SARS-CoV fluorescent VLPs. Viral proteins from cell lysates (left panel) and sedimented VLPs from medium (right panel) were analyzed by Western blot. VLPs could be produced when either N or S (lanes 9 and 10) but not M (lane 8) were tagged with fluorescent proteins. **B.** Production of fluorescent VLPs and efficiency of incorporation of NeCFP and SeYFP fusion proteins into VLPs. Cells were co-transfected with the specified plasmid combinations (corresponding to lanes 9 and 10 of panel A) and purified VLPs from medium were analyzed by sucrose gradient. Tagging S (lower blot) resulted in a greater yield of VLP production when

1040 compared to tagged N (upper blot). However, the eYFP tag greatly reduced S
1041 incorporation onto VLPs (lower blot). Arrows indicates spike trimers and
1042 monomers.
1043
1044 **Figure 6. Tracking of fluorescent SARS-CoV VLPs in living cells. A.** Widefield
1045 fluorescence microscopy images showing accumulation of fluorescent VLPs at the
1046 plasma membrane of pIRES-M-E plus pcDNA-NeCFP co-transfected cells (panels
1047 b), whereas a strong perinuclear staining was observed in Vero E6 expressing
1048 NeCFP alone (panel a). **B.** Confocal microscopy of living cells expressing M-E-
1049 NeGFP VLPs. Four categories of fluorescent signals were observed: a bright and
1050 static large perinuclear compartment (white encircling lines), smaller and dimmer
1051 actively trafficking vesicles (orange encircling lines), bright dots accumulating at
1052 the cell cortex (yellow encircling lines) and dots in the medium surrounding
1053 transfected cells (yellow dots). Videos are available as Supplemental Material. **C.**
1054 Treatment of transfected cells with brefeldin A (BFA) alters trafficking of
1055 fluorescent vesicles. Vero E6 cells were transfected with pIRES-M-E plus pcDNA-
1056 NeGFP plasmids. Cells were either non-treated (a) or treated with 6μg/ml of BFA
1057 for either 4 hours (d) or overnight (g). BFA was then added to non-treated cells
1058 and time-lapse acquisitions were performed. Panels b and c show the same cell
1059 than in panel a but after 25 and 70 minutes incubation with the drug. Alternatively,
1060 BFA was washed out and recovery after BFA treatment was analysed (panels e, f
1061 and h, i). Panels a, b and c, d and e, g and h show same cells at different time
1062 points. Video illustrating panels b, d, f, h and I are provided as supplementary
1063 data.
1064

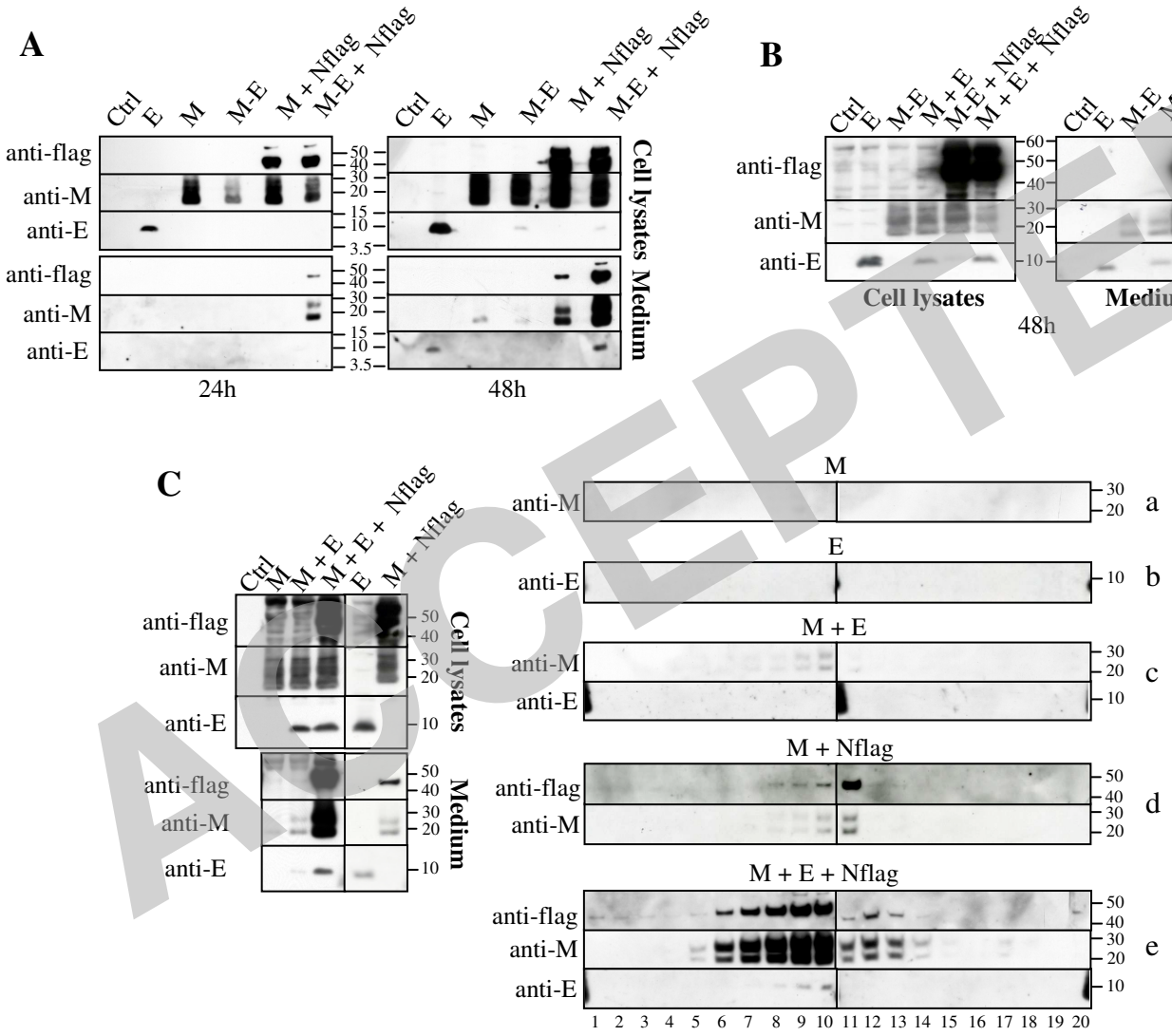

Figure 1

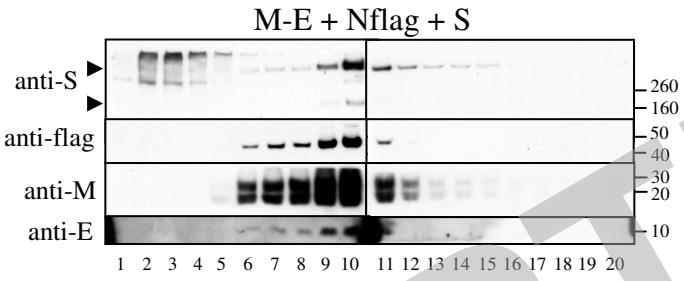

Figure 2

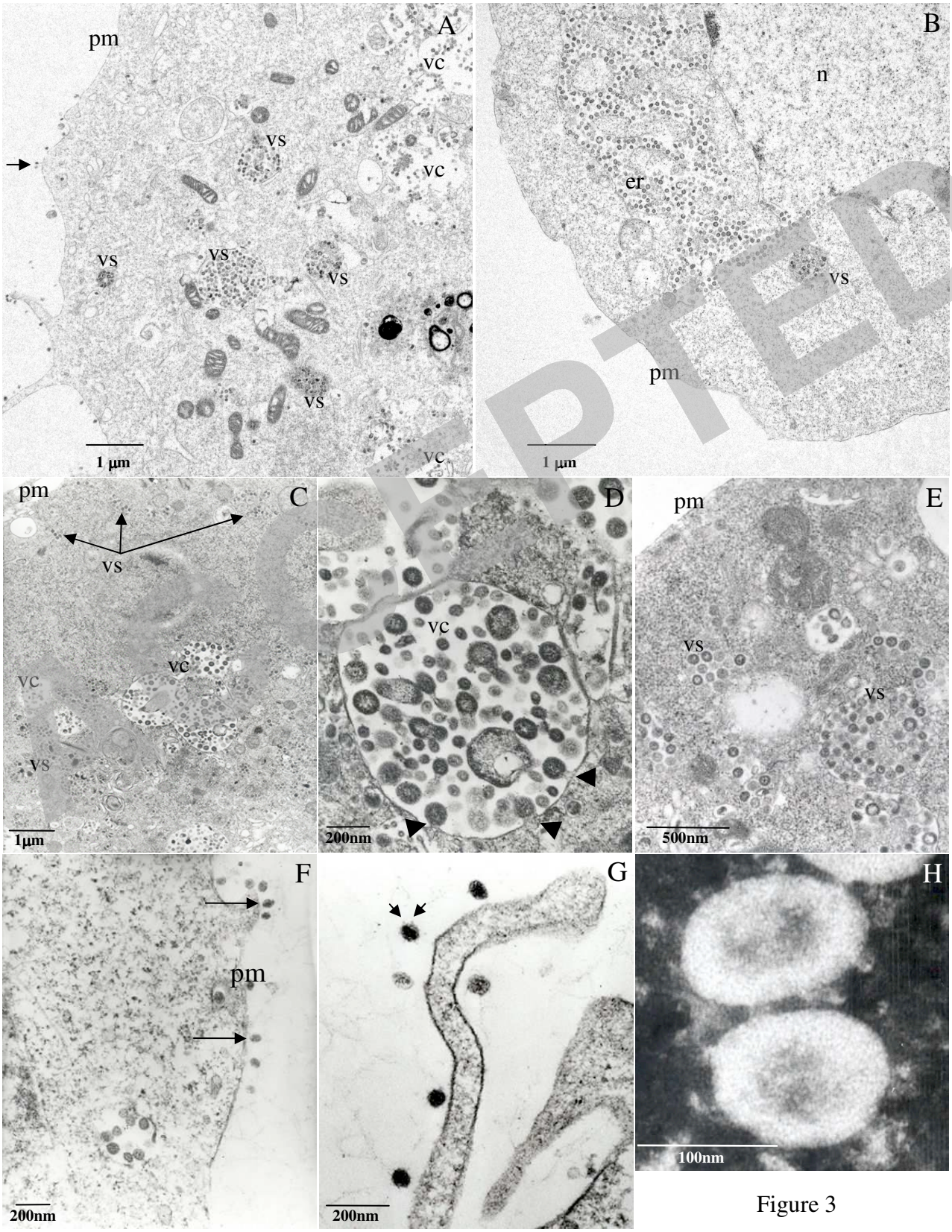

Figure 3

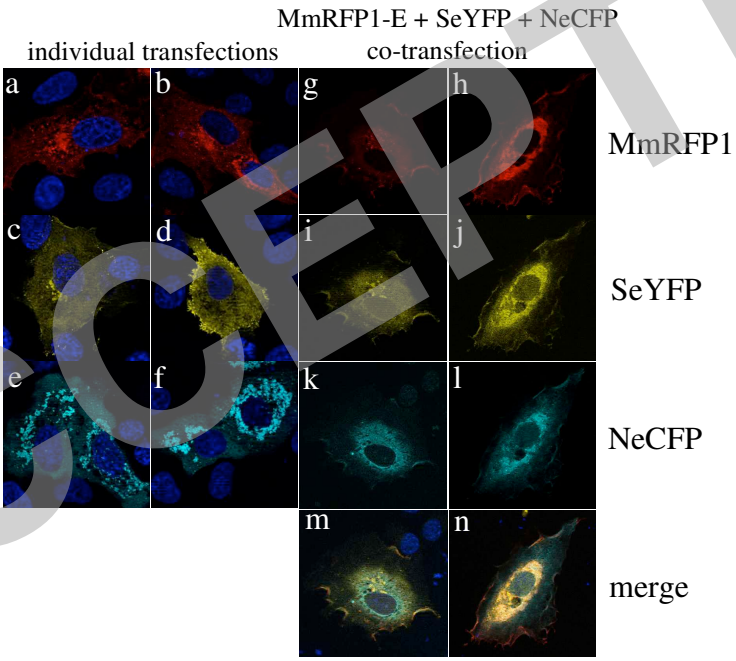

Figure 4

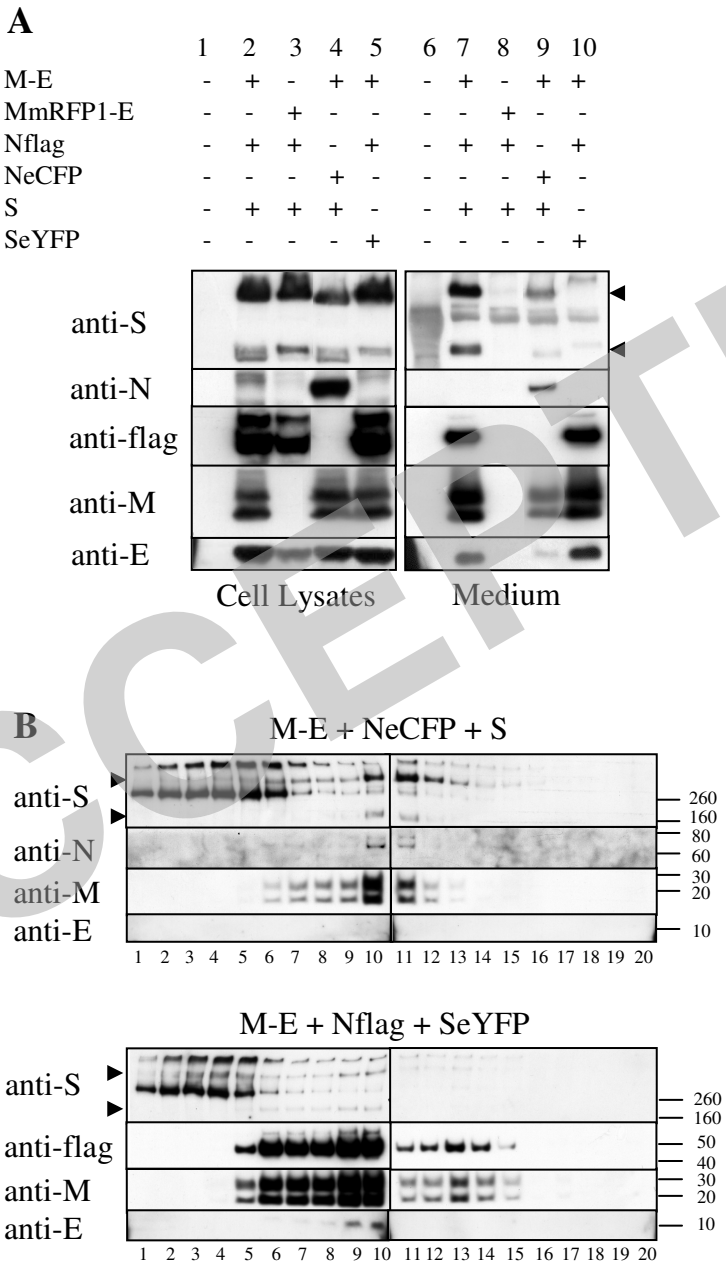

Figure 5

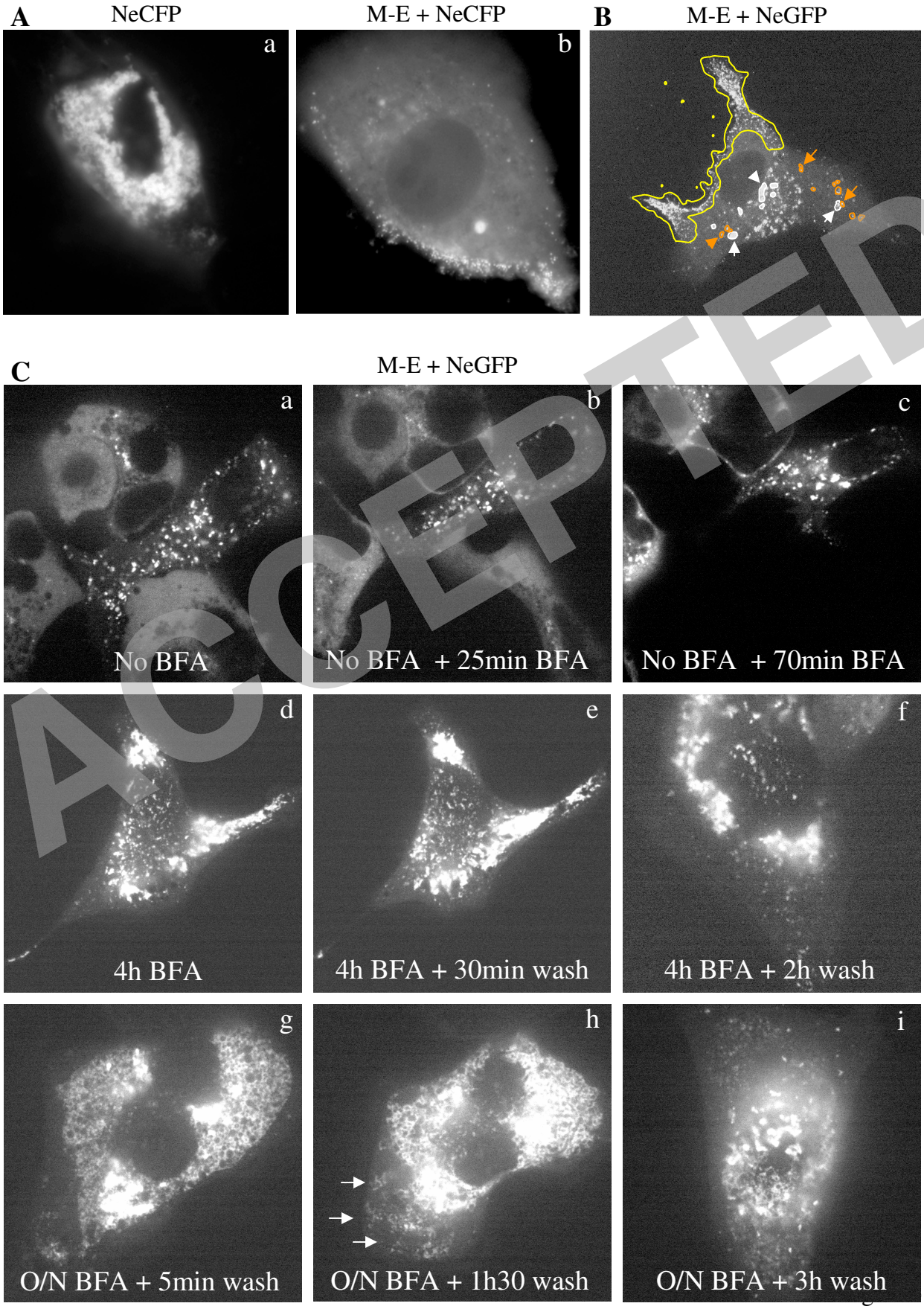

Figure 6